IOPscience iopscience.iop.org

Home Search Collections Journals About Contact us My IOPscience

Magnetically induced ferroelectricity in $TbMnO_3$: inverse Goodenough–Kanamori interaction

This article has been downloaded from IOPscience. Please scroll down to see the full text article.

2009 J. Phys.: Condens. Matter 21 064203

(http://iopscience.iop.org/0953-8984/21/6/064203)

View the table of contents for this issue, or go to the journal homepage for more

Download details:
IP Address: 129.252.86.83
The article was downloaded on 29/05/2010 at 17:45

Please note that terms and conditions apply.

J. Phys.: Condens. Matter **21** (2009) 064203 (7pp) doi:10.1088/0953-8984/21/6/064203

Magnetically induced ferroelectricity in $TbMnO_3$: inverse Goodenough–Kanamori interaction

Kunihiko Yamauchi and Silvia Picozzi

Consiglio Nazionale delle Ricerche—Istituto Nazionale per la Fisica della Materia (CNR-INFM), CASTI Regional Laboratory, 67100 L'Aquila, Italy

E-mail: silvia.picozzi@aquila.infn.it

Received 27 June 2008, in final form 8 September 2008
Published 20 January 2009
Online at stacks.iop.org/JPhysCM/21/064203

Abstract

Improper ferroelectricity in magnets, as induced by non-centrosymmetric spin-, charge- or orbital-ordering, is a branch of the field of multiferroics having fascinating physics and a potentially important technological outcome. We focus here on ferroelectricity in orthorhombic $TbMnO_3$, where the magnetic field along the a-axis produces a polar collinear spin-arrangement with a rather large in-plane electric polarization. The mechanism, similar to that occurring in orthorhombic $HoMnO_3$ in the AFM-E phase, is efficiently driven by a large modification of the structural properties (such as MnO bond-lengths and Mn–O–Mn bond-angles) to favor e_g electron hopping between Mn with parallel spins. A similar mechanism where the t_{2g} states are involved is examined through a hypothetical collinear spin-structure, resulting in a weaker out-of-plane ferroelectric polarization.

(Some figures in this article are in colour only in the electronic version)

1. Introduction

Long-range dipolar and magnetic orders coexist in advanced multifunctional materials called multiferroics [1–4]. In this field, what triggers the currently high level of interest is not just the coexistence but rather the coupling between these two kinds of order. The latter is often referred to as magnetoelectricity, i.e. cross-coupling phenomena through which magnetic (ferroelectric) properties can be induced or switched or tuned via an electric (magnetic) field. Unfortunately, magnetoelectric effects have proven so far to be rather weak in prototypical multiferroic compounds (i.e. $BiFeO_3$, $BiMnO_3$), hindering their large-scale applications. Recently, another class of multiferroics have emerged, in which the ferroelectric transition is often referred to as 'improper' [2, 5, 6]: in the latter case, the primary order parameter is related to a spin, charge or orbital phase transition where the ordered state lacks inversion-symmetry (IS), paving the way to ferroelectricity. The appealing aspect of improper magnetic ferroelectrics (IMF) is that the coupling between, say, magnetism and ferroelectricity is intimate, since both phenomena share a common origin. In closer detail, ferroelectricity is obtained as a by-product of a magnetic transition, since it is the spin degrees of freedom that induce spontaneous electric polarization.

We recall that improper ferroelectricity (IFE) is at variance with its 'proper' counterpart: in standard perovskite-like displacive ferroelectrics, the only phase transition that occurs is related to ionic displacements (of the order of 0.1 Å: for Ti off-center in prototypical $BaTiO_3$) with respect to a centrosymmetric atomic arrangement, giving rise to a permanent polarization which is switchable with an electric field. At variance with the latter case, in IMF, there can be a finite ferroelectric (FE) polarization even without ionic displacements or, in other words, with the atoms in a centrosymmetric arrangement: purely electronic effects can in fact cause the loss of IS and give rise to ferroelectricity. Moreover, we note that what drives the FE transition in standard proper perovskites is covalency: Cohen [7] has shown that, in $BaTiO_3$, apical O p states efficiently hybridize with empty Ti d states resulting in a sizeable energy gain upon FE distortion. On the other hand, in IMF, the spin or charge or orbital transition is mainly driven by correlation effects, i.e. due to strong Coulomb repulsion in localized d or f shells, the behavior of each electron in the solid is strongly affected by

 © 2009 IOP Publishing Ltd Printed in the UK

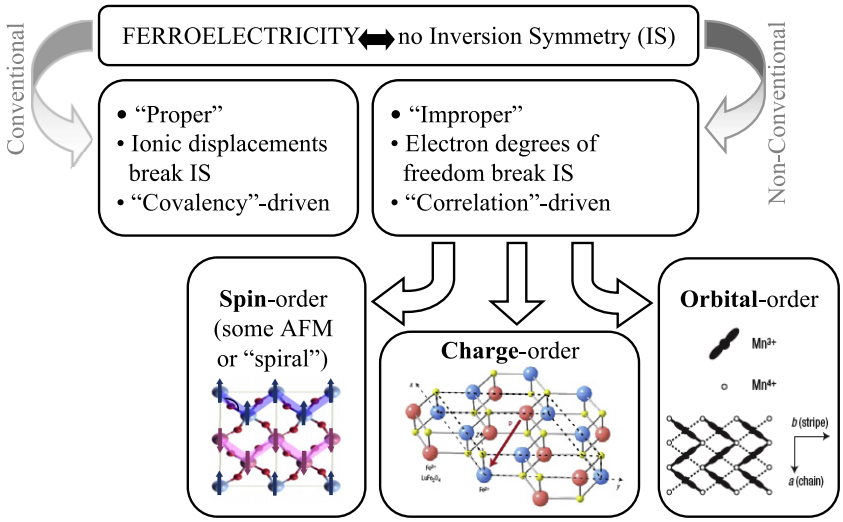

Figure 1. Schematics of IFE in magnets as caused by breaking of IS by non-centrosymmetric spin-, charge- or orbital ordering. The differences with respect to standard ferroelectrics are also highlighted. As examples of materials where this kind of mechanism efficiently occurs, we show in the insets a schematic representation of orthorhombic $HoMnO_3$ (adapted from [8]), $LuFe_2O_4$ (adapted from [2] and [9]) and $Pr(Sr_{0.1}Ca_{0.9})_2Mn_2O_7$ (adapted from [10]).

that of the other electrons. The introductory issues discussed so far are summarized and schematically illustrated in figure 1.

Recently, several *ab initio* studies based on density functional theory have been devoted to IMF, ranging from collinear non-centrosymmetric antiferromagnets [8, 11] to spin-spiral Dzyaloshinskii–Moriya induced ferroelectricity [12–14], from non-centrosymmetric charge-ordering arrangements [15] to doped manganites, where it is the interplay between charge, spin and orbital ordering that induces an electric polarization [16]. In this work, we will focus on collinear spin-arrangements in terbium manganite, along the line of our previous works focused on collinear E-type antiferromagnetic (AFM) $RMnO_3$ [17] where we clarified the microscopic mechanism for ferroelectricity, by using the newly developed Wannier function method. It was shown that, as a result of the peculiar E-type spin-configuration, the asymmetric hopping of Mn-e_g electrons plays an important role in the IFE in the MnO_2 plane. In this work, we will consider improper ferroelectricity as induced in-plane upon application of a magnetic field to $TbMnO_3$. We recall that, in its ground state, $TbMnO_3$ shows an incommensurate spin-spiral arrangement, with the wavevector characterizing the modulation of the Mn spins of $(k \pm \delta, 0, 0)$, where $\delta \sim 0.29$ below T_N and ferroelectric polarization along the b-axis (in the *Pnma* setting). However, under a magnetic field applied along the a-axis, a modulation of $\delta = \frac{1}{4}$ describes the Mn spins and the polarization direction flips to the c-axis [18]. Whereas first-principles calculations have been recently performed for $TbMnO_3$ in the spin-spiral ground state (where spin–orbit coupling (SOC) as related to an 'inverse' Dzyaloshinskii–Moriya interaction is invoked as a source for ferroelectricity) [14, 13], we here focus on the collinear field-induced magnetic ground state and focus on a sort of 'inverse' Goodenough–Kanamori (iGK) interaction [19] as causing the ferroelectric state. By iGK, we mean the modification of the structural properties (in terms of MnO bond-lengths and Mn–O–Mn bond-angles), when imposing a certain spin-arrangement. Within this same framework, in the last part we will focus on the efficiency of the t_{2g} versus e_g orbitals in inducing ferroelectricity, by examining a hypothetical spin-configuration that can give an out-of-plane polarization.

2. Magnetic structure and computational details

The unit cell in orthorhombic $TbMnO_3$ shows *Pnma* symmetry, with strong distortions with respect to the ideal cubic perovskite [20–23]. In order to investigate magnetically driven ferroelectricity, we have considered four types of AFM configuration: AFM-A, AFM-E, AFM-E^b and AFM-E^{4a}, as shown in figure 2. AFM-A and AFM-E are named after the standard Wollan–Koehler notation [24], with AFM-A showing FM (AFM) intraplanar (interplanar) coupling and AFM-E showing in-plane FM zig-zag chains antiferromagnetically coupled to the neighboring chains and an AFM interplanar coupling. The AFM-E^{4a} configuration is taken from the experimental model proposed in [18], which mimics the spin alignment under a magnetic field above a critical value $H > H_{crit}$ along the a-axis [18]. In this situation, the originally non-collinear spins in the spiral state are aligned by the field along the a-axis in the $4a$ periodicity (note that the direction of the spin moment with respect to the lattice is not relevant in our simulations, since SOC is neglected so that the spin and lattice degrees of freedom are decoupled). When focusing on the FM zig-zag chains, AFM-E^{4a} is a 'doubled' AFM-E configuration: according to a mechanism similar to the 'single' AFM-E [25, 8] and based on the inequivalency of the oxygen atoms when bonded to Mn with parallel or antiparallel spins, AFM-E^{4a} might show a FE polarization along the c-axis. The AFM-E^b configuration is a hypothetical spin-arrangement, designed to examine the effects of the iGK as a source of improper FE along the b-axis. The AFM-E^b shows the same intraplanar coupling as the AFM-E configuration, but the phase of the FM zig-zag

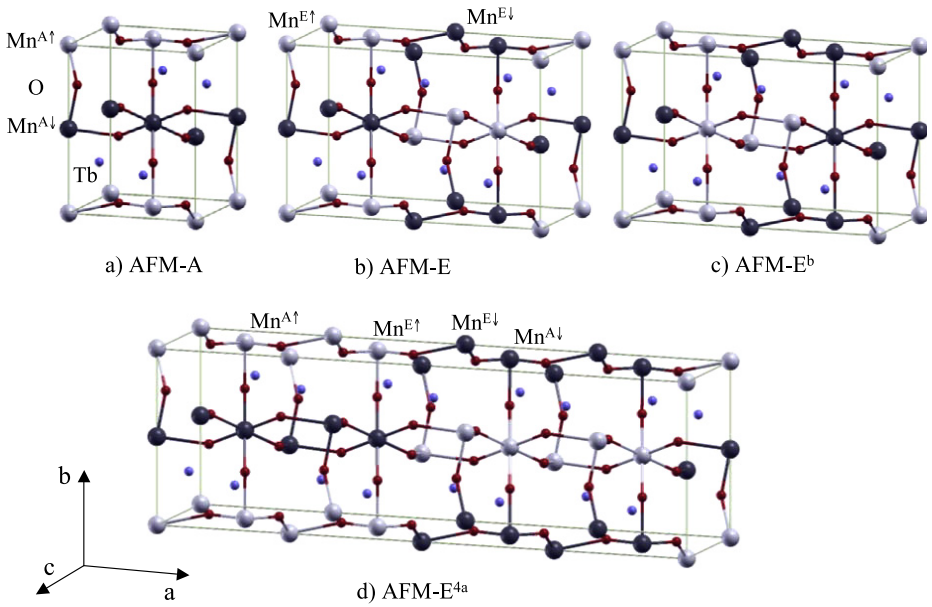

Figure 2. Antiferromagnetic configurations in (a) AFM-A, (b) AFM-E, (c) AFM-E^b and (d) AFM-E^{4a}. Large white and black balls indicate up- and down-spin Mn sites, respectively. Small (red) balls bonded to Mn atoms denote O ions, whereas isolated small (blue) balls denote Tb.

chains is shifted on alternating MnO_2 planes. As a result, there are FM chains showing a zig-zag pattern along the b-axis too. From the point of view of space group operations, there are eight symmetry operations in the non-magnetic $Pnma$ group: E, $\{C_{2x}|\frac{1}{2}\frac{1}{2}\frac{1}{2}\}$, $\{C_{2y}|0\frac{1}{2}0\}$, $\{C_{2z}|\frac{1}{2}0\frac{1}{2}\}$, I, $\{\sigma_x|\frac{1}{2}\frac{1}{2}\frac{1}{2}\}$, $\{\sigma_y|0\frac{1}{2}0\}$, $\{\sigma_z|\frac{1}{2}0\frac{1}{2}\}$. These are reduced as follows in the AFM configurations: E, C_{2z}, I, σ_z at AFM-A; E, C_{2z}, σ_x, σ_y at AFM-E and E^{4a}; E, C_{2z} at AFM-E^b phase. Therefore, by symmetry, only P_z is allowed in the AFM-E and E^{4a} phases, whereas all three components P_x, P_y and P_z are allowed in the AFM-E^b phase. The AFM-A spin-arrangement, which contains the space-inversion as a symmetry operation, is taken as reference for a paraelectric state.

The calculations were done by using the Vienna *Ab initio* Simulation Package (VASP), [26] with the projector-augmented-wave (PAW) potential [27] and the Perdew–Becke–Erzenhof parametrization [28] in the generalized gradient approximation to the exchange–correlation potential. The plane wave cut-off is set to 400 eV. We used eight special k-points (divided as $4 \times 3 \times 4$) in a 1/8 irreducible Brillouin zone (IBZ) for the AFM-A phase, four k-points ($2 \times 3 \times 4$) in 1/4 IBZ for the AFM-E phase, four k-points ($1 \times 3 \times 4$) in 1/4 IBZ for the AFM-E^{4a} phase and eight k-points ($2 \times 3 \times 4$) in 1/2 IBZ for the AFM-E^b phase, according to the Monkhorst–Pack scheme [29]. The experimental lattice parameters [23] were used and the internal parameters of the atomic structure were fully optimized in each AFM phase. The Berry phase for polarization [30] was calculated by integrating over the k-point strings in the plane parallel to the b and c axes, where each string contains six k-points. The density of states (DOS) was calculated in a finer k-point mesh ($8 \times 6 \times 8$ mesh for the AFM-A phase). The localized R-4f electrons are considered as 'core' electrons. Other details are the same as in our previous papers [8, 17].

3. Inverse Goodenough–Kanamori interaction

Before we discuss our results, let us introduce the iGK interaction carefully. According to the original Goodenough–Kanamori rules [31], the dependence of the magnetic coupling on the Mn–O–Mn angle ϕ is explained through kinetic and direct exchange. Between two electrons at different sites, it is known that kinetic exchange occurs when the two orbitals are overlapped, whereas direct exchange (also called 'potential exchange') occurs when the two orbitals are orthogonal. Within kinetic exchange, an electron on one site hops onto the neighboring site which is occupied by electrons with an opposite spin, so that the magnetic coupling is antiferromagnetic. On the other hand, direct exchange is the extension of Hund's rule, so that the coupling becomes ferromagnetic. Since kinetic exchange is usually stronger than direct exchange, here we consider only kinetic exchange between Mn and O sites, i.e. we consider only the bonding orbitals between the two atoms. The magnetic coupling between Mn d electrons via O p strongly depends on the d-orbital configurations and on the Mn–O–Mn angle ϕ. In order to consider the Mn–O–Mn superexchange interaction in $TbMnO_3$, we focus on the interaction between occupied Mn-e_g ($d_{3x^2-r^2}$ and $d_{3y^2-r^2}$) (showing orbital ordering in the ac-plane) and Mn-t_{2g} orbitals; the latter ones interact in both the ac and bc planes (see section 4). These relevant interacting orbitals are schematized in figure 3. Hereafter, we assume the first Mn atom (Mn_1) to have an up-spin d electron, and we discuss the coupling with the second Mn atom (Mn_2) via the O p state. First consider the Mn-e_g orbitals with $\phi = 180°$ (figure 3(a)). In this case, the kinetic exchange aligns both the Mn_1 d–O p_x and O p_y–Mn_2 d spins in an antiferromagnetic configuration; at the same time, the Hund coupling aligns p_x and p_y spins ferromagnetically at the O site. As a result, the Mn_1 and Mn_2 spins are aligned ferromagnetically. In the case

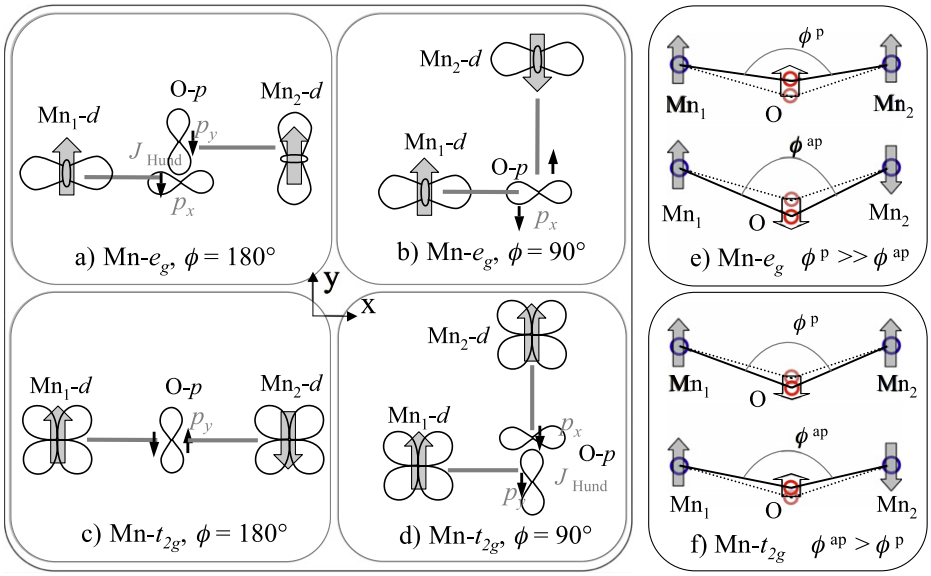

Figure 3. Schematic pictures of (a)–(d) Goodenough–Kanamori interaction between Mn d spins via O p electrons and (e), (f) inverse Goodenough–Kanamori interaction which causes atomic displacement. See the text for details.

of $\phi = 90°$ (figure 3(b)), only the O p_x electron mediates the superexchange so that the p_x electron is polarized as an up-spin state towards Mn_1 and as a down-spin state towards the other Mn_2 ion. This results in an antiferromagnetic spin-coupling between Mn_1 and Mn_2 d electrons. Now, consider the t_{2g} orbitals: the superexchange interaction shows an opposite nature because of the isotropic symmetry of t_{2g} orbitals. By analogy to the above e_g case, the t_{2g} magnetic coupling results in antiferromagnetically aligned Mn when $\phi = 180°$ and ferromagnetically aligned Mn when $\phi = 90°$ (figures 3(c) and (d)). To conclude, Goodenough–Kanamori interactions cause ferromagnetic (antiferromagnetic) coupling between Mn-e_g (t_{2g}) orbitals at $\phi = 180°$, and antiferromagnetic (ferromagnetic) coupling at $\phi = 90°$.

Next, let us consider the *inverse* Goodenough–Kanamori interaction. Assume a ferro or antiferromagnetic superexchange coupling to be imposed on a Mn–O–Mn molecule with an angle ϕ ranging between 90° and 180°. Then, in order to reduce the magnetic coupling energy, the Mn and O atoms move so as to change the angle ϕ in such a way that the Goodenough–Kanamori interaction is satisfied. That is to say, between e_g (t_{2g}) orbitals, a ferromagnetic Mn–O–Mn bonding tends to increase (decrease) ϕ, whereas an antiferromagnetic Mn–O–Mn bonding tends to decrease (increase) ϕ (figures 3(e) and (f)). This effect, i.e. the iGK interaction, is the driving force that stabilizes an improper ferroelectric polarization when the crystal symmetry is broken along the direction of polarization. Since the Mn-e_g:$d_{3x^2-r^2}$ and the O p_x orbitals make a stronger σ bond than the π bond between the Mn-t_{2g}:d_{xy} and the O p_y orbitals, the contribution from the e_g superexchange is expected to be dominant in the MnO_2 plane, where the e_g orbital is ordered. However, one can expect that the t_{2g} contribution survives in the inter-plane Mn coupling, where the e_g contribution can be neglected. In the following sections, we will show how the iGK interaction occurs in $TbMnO_3$ by imposing different AFM configurations on the Mn atoms.

Table 1. Polarization (in μC cm^{-2}) based on the point charge model, induced by the atomic displacements in the ferroelectric phase of AFM $TbMnO_3$ with respect to the centrosymmetric AFM-A phase: the first four rows show the contribution of Tb, Mn, apical O (O^{ap}), and in-plane O (O^{ip}), respectively, whereas their sum is shown in the fifth row. The polarization calculated by using the Berry phase approach is reported in the last row.

	AFM-E	AFM-E^{4a}	AFM-E^{b}
P_{PCM} (Tb)	(0, 0, −0.40)	(0, 0, −0.24)	(0, 0.056, 0)
P_{PCM} (Mn)	(0, 0, −0.85)	(0, 0, −0.40)	(0, 0.063, 0)
P_{PCM} (O^{apical})	(0, 0, 0.53)	(0, 0, 0.29)	(0, 0.004, 0)
P_{PCM} ($O^{in-plane}$)	(0, 0, −1.36)	(0, 0, −0.72)	(0, 0.076, 0)
Total P_{PCM}	(0, 0, −2.08)	(0, 0, −1.07)	(0, 0.20, 0)
Total P_{BP}	(0, 0, −6.46)	(0, 0, −3.11)	(0, 0.20, 0)

4. Magnetically induced ferroelectricity

Table 1 summarizes the calculated polarization in $TbMnO_3$, both in the point-charge-model (PCM, i.e. considering nominal charges located on the fully-relaxed ions, such as Tb^{3+}, Mn^{3+} and O^{2-}) and in the Berry phase approach. Table 1 shows that the ferroelectric polarization is induced along the *c*-axis in AFM-E and AFM-E^{4a} phases and along the *b*-axis in the AFM-E^{b} phase. In each case, the in-plane oxygen displacement is the dominant contribution to P_{PCM}, followed by the manganese contribution. As shown in [17], the *asymmetric* e_g-electron hopping mainly drives the polarization in AFM-E manganites; therefore, as expected, the net polarization calculated by the Berry phase approach P_{BP} is almost three times larger than P_{PCM} in the AFM-E and AFM-E^{4a} phases. However, we note that P_{BP} has the same value as P_{PCM} in the AFM-E^{b} phase. This will be discussed in greater detail in the following section 4.3.

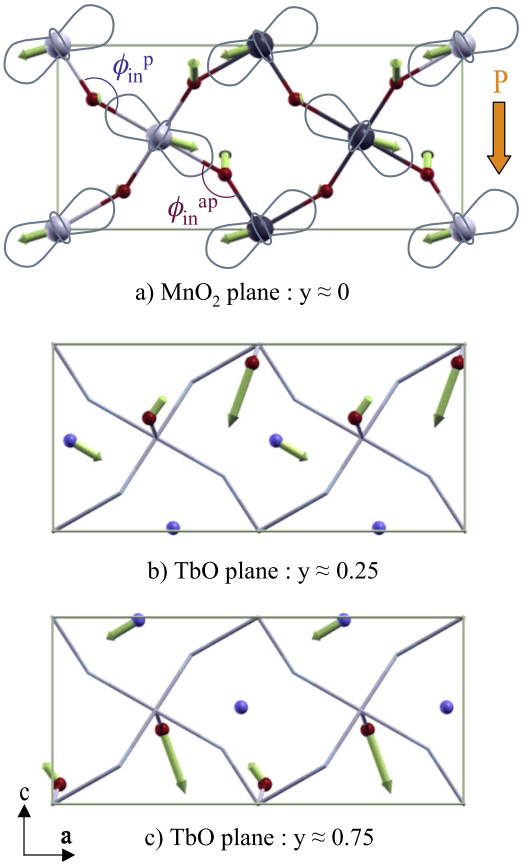

Figure 4. Arrows denote atomic displacements in the *ac* planes of AFM-E $TbMnO_3$ at different *y* coordinates along the *b*-axis. The atomic notation is the same as in figure 2. For clarity in the picture, arrows are magnified by a factor of 1000 with respect to the actual displacement. A schematic representation of the e_g orbital ordering and the direction of the net FE polarization is also shown in panel (a).

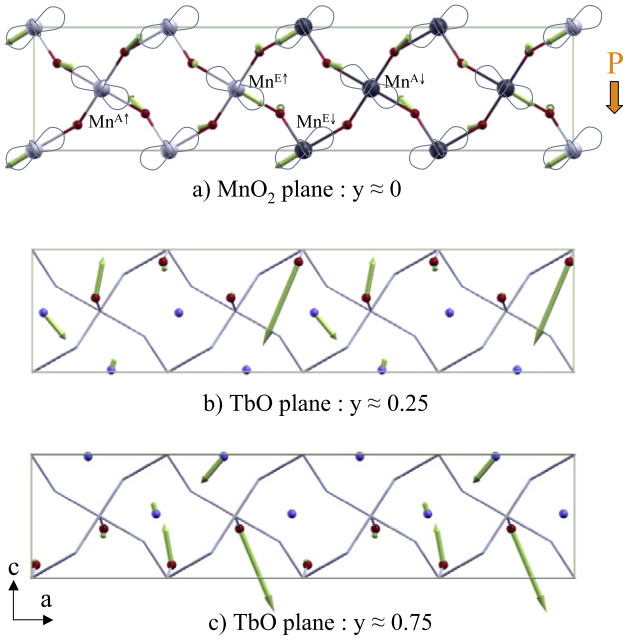

Figure 5. Arrows denote atomic displacements in the *ac* planes of AFM-E^{4a} $TbMnO_3$ at different *y* coordinates along the *b*-axis. The notation is the same as in figure 4.

4.1. AFM-E

The total P_{PCM} and P_{BP} have already been reported and discussed at length in our previous study [17]; we briefly recall here the mechanism leading to those values. The in-plane Mn and O atoms are displaced in order to enhance the asymmetric e_g-hopping so as to increase the in-plane Mn–O–Mn angle with parallel spins ($\phi_{in}^{p} = 146.51°$) and decrease the counterpart with antiparallel spins ($\phi_{in}^{ap} = 143.16°$) shown in figure 4(a). The effect is consistent with what is expected on the basis of the iGK mechanism. It is clear that the e_g contribution is much larger than the t_{2g} contribution in the *ac* plane as discussed in the previous section, so that the Mn ferromagnetic superexchange increases ϕ_{in}^{p} and the Mn antiferromagnetic superexchange decreases ϕ_{in}^{ap}.

At the same time, the in-plane displacements induce a distortion of the Mn-O_6 octahedron. As shown in figures 4(b) and (c), the apical oxygen and terbium atoms are affected by the shift of the in-plane atoms. Note that, because of the mirror symmetry σ_y is left in the symmetries of the AFM-E phase and the *y*-components of the atomic displacements cancel each other.

4.2. AFM-E^{4a}

The AFM-E^{4a} configuration can be considered as half-a-cell wide spin-up and spin-down 'domains', alternating along the *a*-axis (cfr figure 5 where vertical 'stripes' of four white Mn are alternated with 'stripes' of four black Mn along *a*). In other words, one can identify two kinds of Mn atom for each spin-up and -down site. The first type of Mn atom is surrounded by four Mn atoms with the same spin, as in the centrosymmetric AFM-A phase, so that we denote it Mn^{A}. The second one is surrounded by two Mn with the same spin and two others with an opposite spin, as in the polar AFM-E phase, so that we denote it Mn^{E}. In the AFM-E^{4a} spin-arrangement, it is expected that the above mentioned FE mechanism due to the iGK interaction, typical of AFM-E, occurs locally at the interface between spin-up and spin-down 'domains' (i.e. in 'AFM-E'-like regions), so that only half of the Mn ions are ferroelectrically active. Indeed, the calculated polarization, along with each atomically decomposed P_{PCM}, is almost half of what is obtained in the AFM-E phase. Another confirmation of the validity of this 'local' picture is shown by the atomic displacements illustrated in figure 5(a): Mn^{E} atoms are moved in the same way as in the AFM-E phase (cfr figure 4), but Mn^{A} atoms basically keep their original position. As for the comparison of the theoretical results with respect to corresponding experimental results, we remark that, although the direction of the polarization is in agreement with what is reported in [18], the size of our polarization is much larger (by almost two orders of magnitude) than what is observed experimentally. The reason for this discrepancy is not clear at present and deserves further investigations. On the theory side, improvements related to the treatment of (i) correlation effects beyond the standard GGA or GGA + U treatment, or (ii) Tb

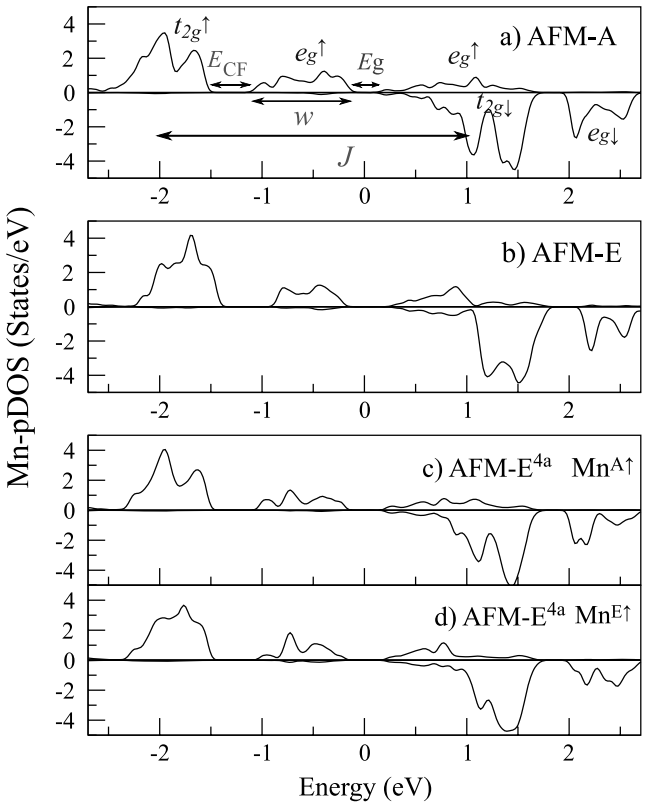

Figure 6. Partial DOS (pDOS) of Mn 3d states in $TbMnO_3$ for (a) AFM-A, (b) AFM-E phase, (c) Mn^A in the AFM-E^{4a} phase and (d) Mn^E site in the AFM-E^{4a} phase. Arrows indicate energy gap (E_g), crystal-field splitting (E_{CF}), bandwidth of the e_g states (w) and on-site exchange interaction energy (J).

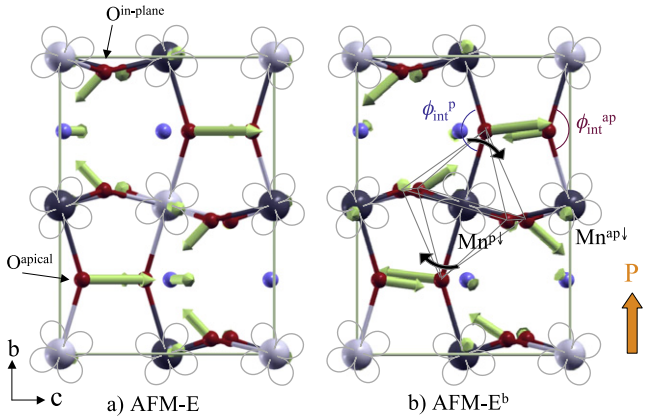

Figure 7. The atomic displacements in the *bc* plane of (a) AFM-E and (b) AFM-E^b $TbMnO_3$. The notation is the same as in figure 2. The schematic arrangement of the out-of-plane t_{2g} states is shown. A Mn-O_6 octahedron is shown, along with the direction of the tilting mode.

atoms where 4f electrons are dealt with in an approximate way, might prove necessary to recover the discrepancy with experiments. On the experimental side, it is not completely clear whether the actual spin-arrangement is indeed collinear and as depicted in [18].

Further insights can be gained when plotting the partial DOS of the Mn sites in the different AFM phases and different spin-environments: the electronic structure of Mn^A and Mn^E in AFM-E^{4a} phase (figures 6(c) and (d), respectively) is compared to their original counterpart in AFM-A and AFM-E phase (figures 6(a) and (b), respectively). As expected, the 3d states of $Mn^{A\uparrow}$ and $Mn^{E\uparrow}$ sites are rather similar to their original 'bulk' analogue. The only significant difference from the $Mn^{A\uparrow}$ state with respect to the corresponding AFM-A phase is the larger energy gap in the larger unit cell (or, correspondingly, the smaller e_g-bandwidth), which is formed by the 1/4 periodicity of the energy potential in the Brillouin zone.

4.3. AFM-E^b

Finally, we discuss the atomic displacements in the E^b phase that induce a polarization along the *b*-axis (cfr table 1). As already observed, P_{BP} has the same value as P_{PCM} and this implies the existence of a different mechanism which causes the FE polarization. This mechanism, which is much more complicated than the in-plane hopping mechanism, can be explained as follows. First, recall that, due to orbital ordering, the e_g orbital lies in-plane and, therefore, the mechanism has to involve something different with respect to the in-plane asymmetric e_g hopping occurring in the AFM-E phase. Let us focus on the inter-plane coordination as well as the magnetic interaction, as compared with that in the AFM-E phase (cfr figure 7). Let us consider the Mn atoms at $y \simeq 0.5$ in the E^b phase: out-of-plane, Mn are coordinated either to two Mn with parallel spins (denoted as Mn^p) or to two Mn with antiparallel spins (denoted as Mn^{ap}). This is of course at variance with the AFM-E phase, where the inter-plane coupling is always AFM. In the E^b phase, the different magnetic configuration causes a different inter-plane Mn–O–Mn angle: $\phi^p_{int} = 142.76°$ in the case of parallel spins and $\phi^{ap}_{int} = 143.19°$ in the case of antiparallel spins. The difference between the angles ($\phi^p_{int} - \phi^{ap}_{int} = -0.43°$) is much smaller than that occurring in-plane ($\phi^p_{in} - \phi^{ap}_{in} = 3.35°$) [8], and notably it has an opposite sign. This is because the in-plane atomic displacements are determined mainly by the double-exchange e_g hopping, whereas the inter-plane displacement is caused by the superexchange interaction of t_{2g} states. In other words, the in-plane iGK interaction is dominated by the e_g orbitals, whereas the inter-plane interaction is dominated by the t_{2g} orbitals so that the in-plane interaction favors 180° angle and the inter-plane interaction favors 90° angle between the parallel-spin Mn atoms. Consequently, the MnO_6 octahedron is more tilted at the inter-plane FM coupling chain and less tilted at the AFM coupling chain. As a result, the tilting slightly cants the direction of the e_g orbital, directed along the long MnO axis, so that the e_g electron hopping from $Mn^{p\uparrow}$ to $Mn^{ap\uparrow}$ and the hopping from $Mn^{ap\uparrow}$ to $Mn^{p\uparrow}$ become different (at variance with the AFM-E case where they all are equivalent). In turn, the O atoms which mediate the interaction between Mn atoms are displaced according to the different e_g hopping and, finally, this gives the net *y* component of the FE polarization. (Note that the position of the O atoms was originally outside the Mn plane: one is upward, one is downward.) The reason

for P_{PCM} showing the same value as P_{BP} probably lies in the fact that the inter-plane t_{2g} superexchange acts only in the direction of tilting the MnO_6 octahedron. However, we do not expect any displacement of the Wannier function center from the atomic center along the *b*-axis, therefore suggesting equivalence between P_{PCM} and P_{BP}.

5. Conclusions

Within the general framework of improper ferroelectric transitions in magnets, as caused by non-centrosymmetric spin-, charge- or orbital-orderings, we focused on collinear spin-arrangements in orthorhombic $TbMnO_3$. In particular, we examined how the inverse Goodenough–Kanamori interaction, which is the driving force of the IFE in the AFM-E phase of ortho-$RMnO_3$, causes an electric polarization in several other AFM configurations. Our calculations predict a rather large polarization along the *c*-axis in the spin-arrangement (labeled as AFM-E^{4a}) obtained upon application of magnetic field along the *a*-axis, which is similar to a 'doubled' AFM-E phase. Due to the peculiar spin-configuration of the AFM-E^{4a} case, the ferroelectricity is explained in terms of the 'local' spin-environment of the Mn atoms: whereas all the octahedrons are ferroelectrically active in the AFM-E phase, only half of the Mn contribute in the AFM-E^{4a} case, with a resulting polarization approximately halved with respect to the corresponding value in AFM-E. Moreover, due to the complicated atomic structure and the symmetry-broken spin-arrangements, we suggest that some AFM phases can induce a weak ferroelectric polarization also along the long *b*-axis, without invoking the Dzyaloshinskii–Moriya interaction caused by the spin–orbit-coupling in the spin-spiral phase.

Acknowledgments

The research leading to these results has received funding from the European Community's Seventh Framework Program (FP7/2007-2013) under grant agreement no. 203523-BISMUTH. Computational support from the CINECA Supercomputing Center (Bologna, Italy) is gratefully acknowledged.

References

[1] Ramesh R and Spaldin N A 2007 *Nat. Mater.* **6** 21
[2] Mostovoy M and Cheong S W 2007 *Nat. Mater.* **6** 13
[3] Khomskii D 2006 *J. Magn. Magn. Mater.* **306** 1
[4] Eerenstein E *et al* 2006 *Nature* **442** 759
[5] Kimura T, Goto T, Shintani H, Ishizaka K, Arima T and Tokura Y 2003 *Nature* **426** 55
[6] Efremov D V, van der Brink J and Khomskii D I 2004 *Nat. Mater.* **3** 853
[7] Cohen R E 1992 *Nature* **358** 136
[8] Picozzi S, Yamauchi K, Sanyal B, Sergienko I A and Dagotto E 2007 *Phys. Rev. Lett.* **99** 227201
[9] Ikeda N *et al* 2005 *Nature* **436** 1136
[10] Tokunaga Y *et al* 2006 *Nat. Mater.* **5** 937
[11] Wang C, Guo G C and He L 2007 *Phys. Rev. Lett.* **99** 177202
[12] Xiang H J and Whangbo M H 2007 *Phys. Rev. Lett.* **99** 257203
[13] Xiang H J *et al* 2008 *Phys. Rev. Lett.* **101** 037209
[14] Malashevic A and Vanderbilt D 2008 *Phys. Rev. Lett.* **101** 037210
[15] Xiang H J and Whangbo M H 2007 *Phys. Rev. Lett.* **98** 246403
[16] Giovannetti G, Kumar S, van den Brink J and Picozzi S, unpublished
[17] Yamauchi K, Freimuth F, Blügel S and Picozzi S 2008 *Phys. Rev.* B **78** 014403
[18] Aliouane N *et al* 2006 *Phys. Rev.* B **73** 020102
[19] Yamasaki Y, Miyasaka S, Goto T, Sagayama H, Arima T and Tokura Y 2007 *Phys. Rev.* B **76** 184418
[20] Zhou J S, Goodenough J B, Gallardo-Amores J M, Morán E, Alario-Franco M A and Caudillo R 2006 *Phys. Rev.* B **74** 014422
[21] Tachibana M, Shimoyama T, Kawaji H, Atake T and Takayama-Muromachi E 2007 *Phys. Rev.* B **75** 144425
[22] Mori T, Kamegashira N, Aoki K, Shishido T and Fukuda T 2002 *Mater. Lett.* **54** 238
[23] Alonso A J, Martinez-Lope M J, Casais M T and Fernandez-Diaz M T 2000 *Inorg. Chem.* **39** 917
[24] Wollan E O and Koehler W C 1955 *Phys. Rev.* **100** 545
[25] Sergienko I A, Sen C and Dagotto E 2006 *Phys. Rev. Lett.* **97** 227204
[26] Kresse G and Hafner J 1993 *Phys. Rev.* B **47** 558
Kresse G and Furthmüller J 1996 *Phys. Rev.* B **54** 11169
[27] Kresse G and Joubert D 1999 *Phys. Rev.* B **59** 1758
[28] Perdew J P, Burke K and Ernzerhof M 1996 *Phys. Rev. Lett.* **77** 3865
[29] Monkhorst H J and Pack J D 1976 *Phys. Rev.* B **13** 5188
[30] King-Smith R D and Vanderbilt D 1993 *Phys. Rev.* B **47** 1651
Resta R 1994 *Rev. Mod. Phys.* **66** 899
[31] Goodenough J B 1955 *Phys. Rev.* B **100** 564
Kanamori J 1959 *J. Phys. Chem. Solids* **10** 87